Magnetic–electronic properties of FeS and Fe_7S_8 studied by ^{57}Fe Mössbauer and electrical measurements at high pressure and variable temperatures

2001 J. Phys.: Condens. Matter 13 10077

(http://iopscience.iop.org/0953-8984/13/44/319)

INSTITUTE OF PHYSICS PUBLISHING JOURNAL OF PHYSICS: CONDENSED MATTER

J. Phys.: Condens. Matter **13** (2001) 10077–10088 PII: S0953-8984(01)23481-X

Magnetic–electronic properties of FeS and Fe_7S_8 studied by ^{57}Fe Mössbauer and electrical measurements at high pressure and variable temperatures

S Takele[1] **and G R Hearne**

School of Physics, University of the Witwatersrand, Private Bag 3, Wits 2050 Johannesburg-Gauteng, South Africa

E-mail: phbsbt@upe.ac.za

Received 29 March 2001, in final form 9 August 2001
Published 19 October 2001
Online at stacks.iop.org/JPhysCM/13/10077

Abstract

The effect of pressure on the magnetic and electronic properties of synthetic FeS and Fe_7S_8 has been investigated by using ^{57}Fe Mössbauer and electrical resistance measurements on polycrystalline samples pressurized in miniature gem anvil cells up to a pressure of ∼12 GPa in the temperature range 300–5 K. FeS in the low-pressure phases ($P \lesssim 7$ GPa) has thermally activated charge carriers and a high-spin electronic configuration along the room temperature isotherm, whereas the high-pressure monoclinic phase ($P \gtrsim 7$ GPa) adopts a magnetically quenched low-spin state and a non-metallic behaviour associated with the filled valence band. The non-metallic behaviour observed in all pressure phases is explained in terms of electron correlation between Fe:3d electrons. In contrast, Fe_7S_8 is magnetic-metallic below ∼5 GPa and diamagnetic-metallic above this pressure. The metallic behaviour is ascribed to hole conduction in the S:3p band, as inferred from the temperature dependence of the Mössbauer data. The collapse of band magnetism at ∼5 GPa in Fe_7S_8 may be due to pressure-induced band broadening, leading to a breakdown of the Stoner criterion.

1. Introduction

The $Fe_{1-x}S$ system is the most widespread monosulfide in nature, crystallizing in a hexagonal or monoclinic structure based on the NiAs-type unit cell. There is usually a substantial deficiency at the cation sites, which may result in solid solutions ranging from the stoichiometric troilite-FeS to the maximum cation deficient pyrrhotite-Fe_7S_8. This cation deficiency is compensated

[1] Present address: Department of Physics, University of Port Elizabeth, PO Box 1600 Port Elizabeth 6000, South Africa.

by vacancies at Fe sites rather than by substituting S atoms in Fe sites, because of atomic size considerations.

Troilite is of interest to both condensed matter and planetary sciences because geophysical arguments suggest that sulfur may be the lighter allowing element in the iron-rich cores of terrestrial planets such as the Earth and Mars [1]. Therefore FeS is the possible component of the interior of these planets. It is also a common mineral in lunar and meteoritic samples [2]. FeS is an antiferromagnetic semiconductor at ambient conditions [3] and is therefore considered to be a strongly correlated electron system, permitting an interesting comparison to be made of such narrow 3d-band phenomena in transition-metal sulfides against those in transition-metal oxides [4]. Pyrrhotite-Fe_7S_8 occurs in sulfide ore deposits of economic interest and it is the only binary sulfide common enough to be considered a rock-forming mineral. It is magnetic-metallic at ambient conditions [3]. The exact origin of the metallic behaviour is, however, not clear.

FeS displays a variety of structural, magnetic and electronic properties at high pressures or temperatures [5, 6]. At ambient conditions, it occurs as a troilite structure; a hexagonal superstructure derivative of the NiAs unit cell having axis lengths of $a = \sqrt{3}a_f$ and $c = 2c_f$ (a_f and c_f are the lattice parameters of a fundamental NiAs sub-cell). The troilite structure ceases to exist at the α-transition and transforms to a new NiAs-type structure at an onset temperature of $\sim$413 K at ambient pressure [2]. This α-transition is typical only to stoichiometric FeS. Upon increasing pressure along the room temperature isotherm it undergoes a structural phase transition to an MnP- [5, 7] or hexagonal-type structure [8] at $\sim$3.5 GPa. Further increase in pressure at ambient temperature results in a structural transition to a monoclinic high-pressure phase.

Although the high-pressure monoclinic phase has been identified by a number of authors [5, 7, 8], its lattice parameters and atomic positions have never been clearly determined until recently by Nelmes *et al* [9] using angle dispersive x-ray powder-diffraction at pressure. They found the same unit cell previously identified by Kusaba *et al* [8] in a structure indexed on a monoclinic unit cell ($a = 8.11$ Å, $b = 5.66$ Å, $c = 6.48$ Å and $\beta = 93.0^\circ$) with space group $P2_{1/a}$ containing 12 formula units.

Fe_7S_8 is a ferrimagnetic metal at ambient conditions with a Néel temperature of 578 K [4, 10]. It has a fundamental NiAs-type hexagonal or monoclinic structure depending on composition and ordering of vacancies [10]. Alternate layers of metal-full and metal-deficient layers stack along the c-axis. Within this superstructure all the magnetic moments in a metal-full layer are aligned parallel and the direction of alignment reverses in moving to the adjacent metal-deficient layer. Exact antiferromagnetic cancellation of atomic moments between two successive layers is thus incomplete, giving rise to a net spontaneous magnetization and consequent ferrimagnetic behaviour.

Previous Mössbauer studies on Fe_7S_8 show that magnetism disappears above a pressure of $\sim$5 GPa at room temperature [6, 11]. No structural symmetry changes have been observed up to a pressure of $\sim$11 GPa at room temperature. However, there is a structural adjustment at the magnetic phase transition at $\sim$5 GPa; the non-magnetic phase being less compressible along the c-axis than the magnetic phase [6].

In these iron sulfide compounds, the variety of crystallographic structures adopted at various high-pressure or high-temperature conditions has been extensively investigated in previous studies, yet the magnetic–electronic properties under high pressure and variable temperatures have been less extensively investigated. Previous attempts have been made but there appears to be ambiguity and speculation in this regard because both the ^{57}Fe Mössbauer-magnetic and electrical transport characterizations have been limited to studies in the vicinity of room temperature [6, 8].

The pressure-induced disappearance of a magnetic signature in the Mössbauer spectrum of FeS at ∼7 GPa at room temperature has been attributed to a collapse of the magnetic moment of the Fe atom, either due to electron delocalization [6] and consequent metallic behaviour, or due to spin-crossover of the Fe atomic spin S from original high-spin $S = 2$ ($Fe^{2+}(3d) : t_{2g}^4\, e_g^2$) to diamagnetic low-spin $S = 0$ ($Fe^{2+}(3d) : t_{2g}^6\, e_g^0$). A drastic change in the magnetic ordering temperature, perhaps to below room temperature, also has to be considered as a possibility due to the pressure-induced decrease in inter-atomic distances and change in bond angles associated with the ∼5% change in unit cell volume at the MnP/hexagonal → monoclinic transition for FeS [8, 9].

A temperature-dependent ^{57}Fe Mössbauer and electrical resistance study to practically accessible low temperatures may help to eliminate any ambiguity regarding both the magnetic–electronic configuration of Fe and the nature of electrical transport in these iron sulfide compounds under pressure. In this paper we present the experimental results of the magnetic and electronic properties of troilite-FeS and pyrrhotite-Fe_7S_8 at high pressure and variable cryogenic temperatures using ^{57}Fe Mössbauer and electrical-resistance measurements. While high-pressure ^{57}Fe Mössbauer studies at room temperature have been reported elsewhere [6] and part of the present results of FeS have been published previously as a brief report [12], this paper focuses only on a detailed analysis of the results obtained at variable low temperatures on both FeS and the cation-deficient Fe_7S_8 for comparison of their magnetic and electronic properties under hydrostatic high pressure.

2. Experimental details

Samples of troilite-FeS and pyrrhotite-Fe_7S_8, isotopically enriched to ∼25% ^{57}Fe, have been synthesized in milligram quantities for high-pressure ^{57}Fe Mössbauer studies by reacting the elements in evacuated quartz tubes for several days. For high-pressure electrical resistance studies, samples were synthesized from natural isotopic materials. Mössbauer spectra under ambient conditions yield almost identical hyperfine interaction parameters to those obtained by Kobayashi *et al* [6] for samples synthesized using natural abundance materials, which they deduced to have a chemical formula of $Fe_{0.999}S$ for troilite and $Fe_{0.874}S$ for pyrrhotite. X-ray diffraction and Debye–Scherrer studies independently confirm the stoichiometry of our materials as being close to $Fe_{0.996}S$ for troilite and $Fe_{0.875}S$ for pyrrhotite.

For ^{57}Fe Mössbauer studies some of the fine powder has been loaded into a 300 μm × 50 μm cavity drilled in $Ta_{90}W_{10}$ gaskets mounted for pressure studies in a miniature Merrill–Basset-type diamond anvil cell (DAC). The shift in R_1 of the ruby luminescence line at room temperature from fine ruby powder loaded into the sample cavity has been used to determine the pressure. Liquid argon was loaded into the sample cavity to ensure a quasi-hydrostatic pressure environment. The pressure distribution in the sample cavity was checked by measuring a number of ruby grains distributed throughout the cavity at room temperature and the average of these pressures was taken as the pressure of the sample. In our resistance–pressure experiments, four-probe current-reversing resistance–temperature (R–T) measurements have been performed with a dip-stick-type arrangement in a storage Dewar using cubic zirconia gems as pressure anvils, fine gold-wire electrodes and insulating mica gaskets to constitute the confining sample cavity [13].

3. Results

^{57}Fe Mössbauer spectra at room temperature recorded at selected pressures for each of the three phases occurring along the room temperature isotherm for FeS and at a pressure of ∼11 GPa

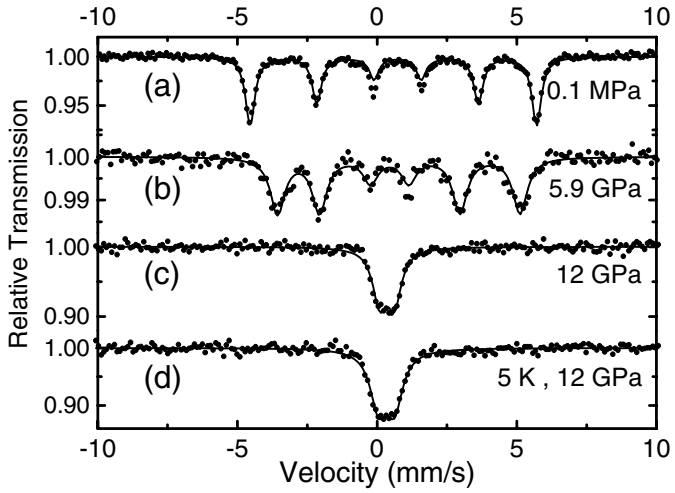

Figure 1. ^{57}Fe Mössbauer spectra of FeS in the three structural phases at elevated pressure: (a) troilite, (b) MnP/hexagonal and (c) monoclinic. Magnetic spectra in (a) and (b) as well as the quadrupole-doublet in (c) at pressure have been recorded at room temperature whereas the spectra in (d) is recorded at 5 K under pressure. The spectra in the monoclinic high-pressure phase in (c) and (d) indicate non-magnetic behaviour both at room temperature and 5 K, respectively. Full circles are data points and full curves are theoretical fits to the experimental data.

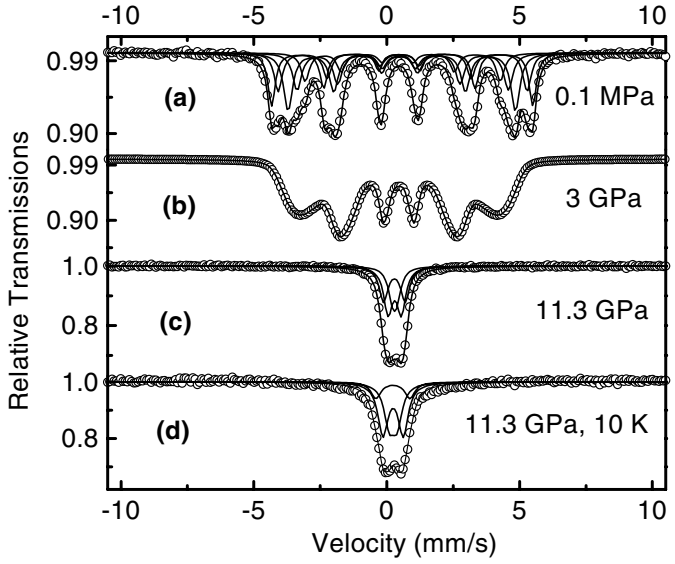

Figure 2. ^{57}Fe Mössbauer spectra of Fe_7S_8 at elevated pressures (a)–(c). Magnetic spectra at pressures in (a) and (b) have been recorded at room temperature, whereas the spectra at higher pressure in (c) and (d) indicate non-magnetic behaviour both at room temperature and 10 K, respectively. Full curves are theoretical fits and open circles are experimental data.

for Fe_7S_8 are shown in figures 1(a)–(c) and figures 2(a)–(c), respectively. The spectra show a collapse of magnetic sextets at room temperature to quadrupole interaction doublets beyond the magnetic transition pressures of $\sim$7 and $\sim$5 GPa for FeS and Fe_7S_8, respectively, in

Table 1. Hyperfine interaction parameters for FeS at 12 GPa and variable cryogenic temperatures. The isomer shift values are with respect to α-Fe at ambient conditions.

T (K)	δ (mm s^{-1})	ΔE_Q (mm s^{-1})
300	0.46 (1)	0.57 (2)
150	0.468 (5)	0.566 (8)
80	0.447 (8)	0.58 (1)
35	0.451 (8)	0.59 (1)
5	0.447 (9)	0.59 (1)

Table 2. Hyperfine interaction parameters for Fe_7S_8 at 11.3 GPa and variable cryogenic temperatures. The isomer shift values are with respect to α-Fe at ambient conditions.

T (K)	δ (mm s^{-1})	ΔE_Q (mm s^{-1})
300	0.401 (4)	0.46 (7)
	0.396 (3)	0.78 (3)
	0.394 (4)	0.15 (3)
85	0.356 (3)	0.53 (3)
	0.341 (4)	0.97 (1)
	0.334 (6)	0.13 (5)
10	0.352 (3)	0.30 (2)
	0.34 (1)	1.28 (4)
	0.350 (3)	0.76 (4)

agreement with previous studies [6, 11]. Our Mössbauer studies of cryogenic temperatures (figures 1(d) and 2(d)) show that the non-magnetic quadrupole doublets persist at the lowest temperature of 5 K for FeS and 10 K for Fe_7S_8, strongly suggestive of diamagnetic behaviour. The possibility that the high-pressure phases have spin-ordering temperatures below 300 K at pressures beyond the magnetic transitions may therefore be discounted.

The analyses of the spectra in figure 2 show that the isomer shift for all magnetic-interaction sextets at ambient pressure is $\sim$0.63 mm s^{-1} and for the quadrupole doublets in figure 2(c) at 11.3 GPa is $\sim$0.40 mm s^{-1} with respect to metallic iron. The quadrupole interaction doublets associated with the different iron sites in the metal-full and metal-deficient layers of the structure at 11.3 GPa all have very similar isomer shift values at any given temperature on cooling down to 10 K (see table 2). The hyperfine interaction parameters for FeS at 12 GPa in table 1 and for Fe_7S_8 at 11.3 GPa in table 2 show that there is not much discernible change in the isomer shifts on cooling at these pressures and these indicate no change in the electronic wavefunctions (electron densities) with temperature.

Normalized resistance–temperature measurements at selected pressures spanning the different structural phases at rising pressure are shown in figure 3 for FeS, indicating that a negative coefficient of resistance $dR/dT < 0$ obtains in both the intermediate-pressure (MnP/hexagonal) and high-pressure (monoclinic) phases. This is indicative of a small band-gap semiconductor, contrary to the speculation of all previous studies restricted to measurements in the vicinity of room temperature that claim intermediate-pressure (3.5–7 GPa) and high-pressure ($P > 7$ GPa) phases to be metallic [6, 8]. The structural phase transition from troilite to MnP/hexagonal phase at $\sim$3.4 GPa is followed by a decrease in the electrical resistance up to the magnetic phase transition at $\sim$7 GPa. However, on transition to the diamagnetic monoclinic phase the resistance was found to increase slightly.

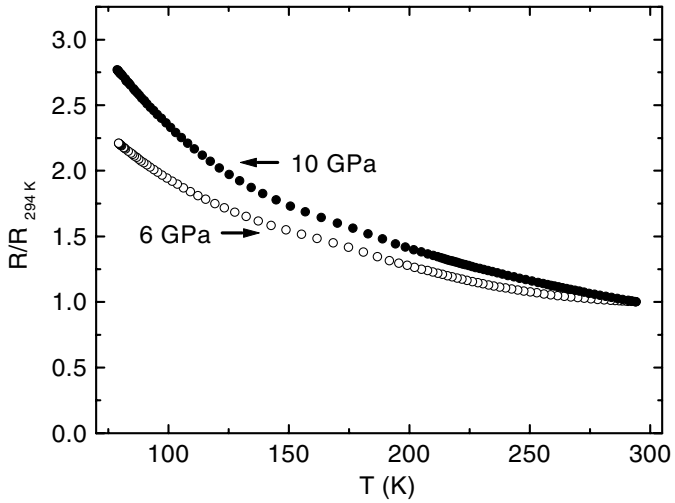

Figure 3. Electrical resistance data of FeS normalized to the resistance value at 294 K at selected pressures in the intermediate MnP/hexagonal and high-pressure monoclinic phases (open and full circles, respectively). The resistance data in both phases indicate non-metallic behaviour.

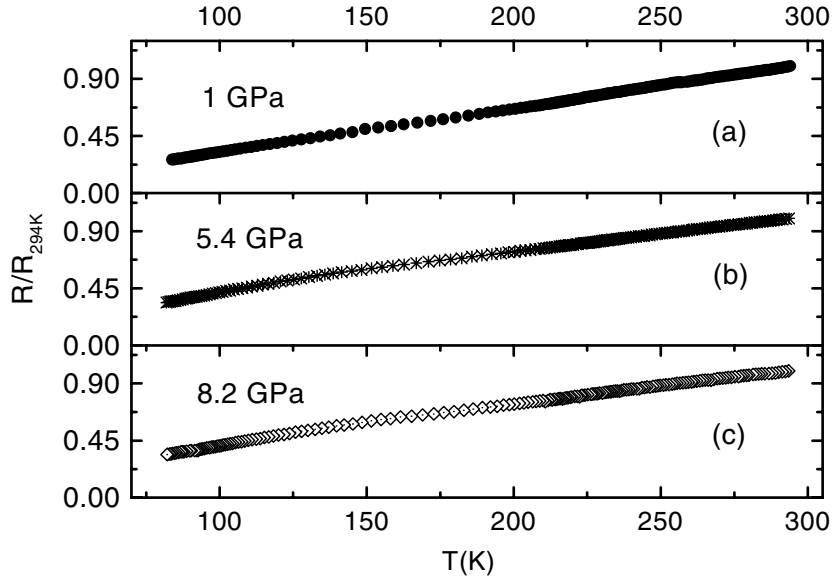

Figure 4. Electrical resistance data of Fe_7S_8 as a function of temperature at selected pressures: (a) in magnetic low-pressure phase at 1 GPa, (b) near the magnetic phase transition at 5.4 GPa and (c) in the diamagnetic high-pressure phase at 8.2 GPa respectively, normalized to the resistance values at 294 K.

In contrast, resistance–temperature measurements on Fe_7S_8 recorded both in the magnetic low-pressure and in the diamagnetic high-pressure phases as well as in the vicinity of the magnetic phase transition (figure 4) show that resistance increases with temperature obtaining a positive temperature coefficient of resistance indicating typical metallic behaviour. Figure 5 shows resistance data of Fe_7S_8 recorded at room temperature and variable pressures. The

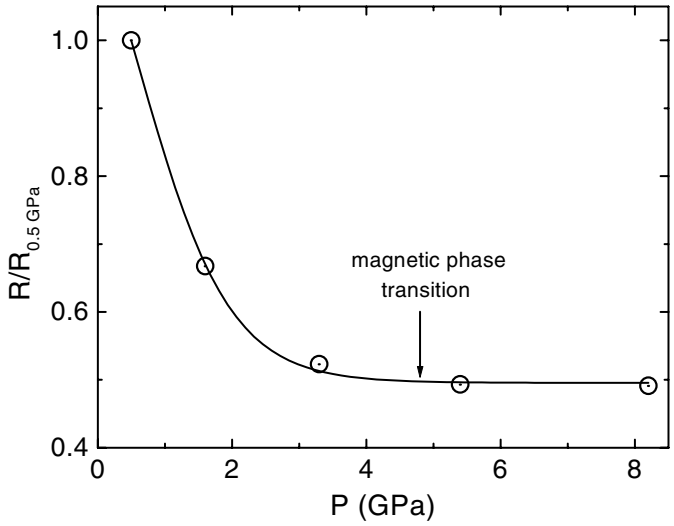

Figure 5. Room temperature electrical resistance of Fe_7S_8 normalized to the resistance value at 0.5 GPa as a function of pressure. Open circles are data points and the full curve is a non-linear fit to the data. The resistance decreases rapidly at low pressures and saturates to an almost constant value for $P \gtrsim 3$ GPa.

resistance decreases very rapidly at low pressures and saturates almost to a constant value beyond ∼3 GPa. No unusual change (increase) in resistance is observed at or near the magnetic phase transition that was observed in FeS.

4. Discussion and conclusions

4.1. Pressure induced spin-crossover and the collapse of magnetism in FeS

From the results of ^{57}Fe Mössbauer and electrical resistance measurements, the magnetic and electronic properties of FeS under pressure along the room temperature isotherm can be classified into two regimes: magnetic non-metallic low-pressure phases ($P \gtrsim 7$ GPa) and diamagnetic non-metallic high-pressure phases ($P \gtrsim 7$ GPa). The non-metallic behaviour observed in all pressure phases with small resistances indicates the activated behaviour of the material; hence the existence of a small but finite energy gap.

Figure 6(a) shows the resistance data of figure 3 plotted in Arrhenius format at 6 GPa in the MnP/hexagonal intermediate-pressure phase and at 10 GPa in the high-pressure monoclinic phase, clearly indicating activated behaviour. The slopes of the Arrhenius plots for both the pressures are not the same. The difference in the slopes suggests a range of activation energies. The activation energies E_A deduced from the Arrhenius plots near room temperature in the range $250 < T < 294$ K are also indicated in figure 6(b).

From the observed trends of electrical resistances and energy gaps with pressure in many materials, the resistances and hence the activation energies are expected to decrease as pressure increases mainly due to overlap of atomic orbitals. Nevertheless, the Arrhenius plots in figure 6(a) clearly show that the activation energy for 10 GPa is greater than that for 6 GPa. The values deduced from the slopes of figure 6(b) in the range $250 < T < 294$ K are ∼10.4 meV at 6 GPa and ∼21.9 meV at 10 GPa. These results indicate that the semiconducting behaviour of the material in the low-pressure magnetic and high-pressure diamagnetic phases is quite different, implying different physical origins of the energy gaps.

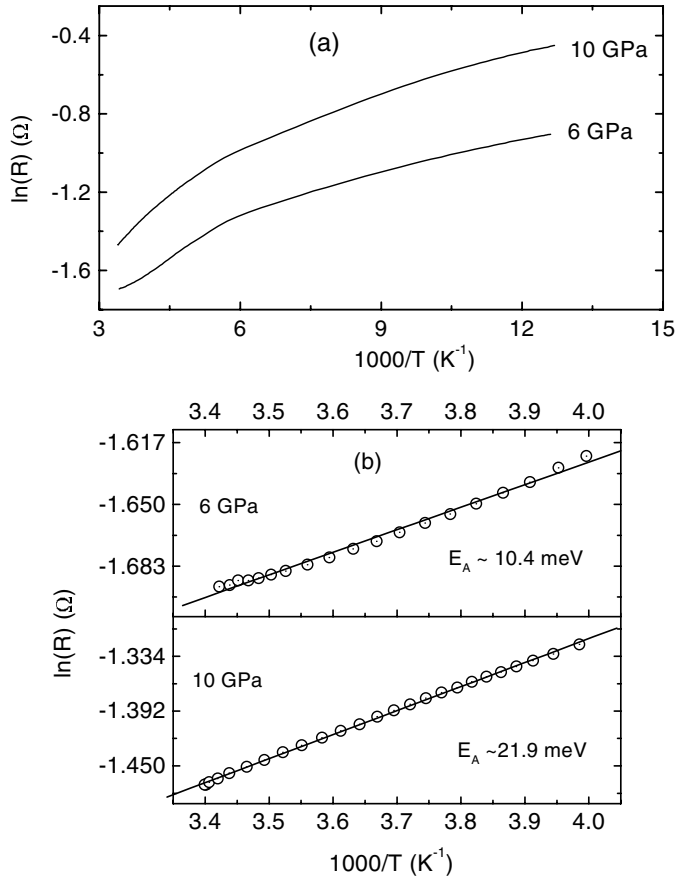

Figure 6. (a) Temperature-dependent resistance of FeS at 6 GPa and at 10 GPa plotted in Arrhenius format showing activated behaviour in both the intermediate MnP/hexagonal and the high-pressure monoclinic phases. (b) Carrier activation energies deduced from the analysis of the data near room temperature in the range 250–294 K. Full curves through the data points in the bottom panel are linear fits to the data.

The theoretical classification of the type of electronic transitions and the alteration of magnetism in transition-metal compounds based on the Zaanen–Sawatzky–Allen scheme [14] are the relative magnitudes of the on-site d–d Coulomb repulsion U, the anion valence band to the cation conduction band charge transfer energy Δ and the bandwidth W. Relative values of Δ and U estimated from configuration-interaction cluster-model calculations [15] categorize FeS in the boundary between charge transfer and Mott–Hubbard insulators where $\Delta \leqslant U$ and U is not very large. In this case, if U is greater than the bandwidth, the d-electrons will have strong enough correlation [16] to introduce spontaneous magnetism and spilt half-filled states into upper Hubbard and lower Hubbard bands [17] leading to a non-metallic ground state.

The non-metallic behaviour in all the pressure phases in FeS, therefore, suggests a localized electron model and associated electron correlation appropriate to this system [4]. Such a system has often been discussed in terms of crystal-field theory [18]. In this case, the magnetic and electrical properties of the system depend on the relative values of the (cation–anion) interatomic crystal field splitting energy between orbitals with the same spin,

Δ_{cf}, and intraatomic (cation: 3d spin pairing) exchange interaction energy, which splits orbitals with different spins, Δ_{ex} [18].

With Fe having an octahedral coordination of six S^{2-} ligands in FeS, the crystal-field splitting Δ_{cf} of ∼1–2 eV represents, within the ligand-field picture, the energy difference between threefold degenerate 3d : t_{2g} and doubly degenerate 3d : e_g orbitals of the cation in the FeS_6 octahedron. Alternatively, Δ_{cf} is a measure of the difference in strength of π-bond and σ-bond cation covalent mixing with ligand orbitals. According to Hund's rule, typical intraatomic exchange stabilization energies Δ_{ex} ∼2–3 eV favour maximal unpaired electron spins and associated orbital occupation to minimize interelectronic repulsion.

With increasing pressure and corresponding reduction of the unit-cell volume, Δ_{cf} may become comparable to or exceed Δ_{ex}. It is then energetically favourable for majority-spin $e_g(\uparrow)$-derived α-electrons to occupy π-bonding orbitals as $t_{2g}(\downarrow)$-derived β-electrons as shown in the evolution of figure 7(b) to figure 7(c) representing the high-spin-to-low-spin spin-pairing transition that leads to a significant alteration of the electronic configuration in the high-pressure monoclinic phase.

The magnetic and non-metallic behaviour of the low-pressure phase ($P \gtrsim 7$ GPa) for FeS suggests a high-spin 3d : $t_{2g}^4\, e_g^2$ cation electronic configuration (see figure 7(b)) and thermally activated charge carriers. The high-spin state has a partially filled minority-spin $t_{2g}(\downarrow)$-derived sub-band contribution to the 3d-valence band, anticipated to lead to the condition $U \to 0$ and render metallic behaviour to FeS in conventional band theory as shown in figure 7(a). Therefore, the non-metallic behaviour must be attributable to a gap ϵ in the $t_{2g}(\downarrow)$ sub-band as indicated in figure 7(b). For both the troilite and MnP/hexagonal phases, which are magnetic semiconductors, the gap may originate either or both from strong electron correlation represented by the Hubbard potential U of the 3d band at narrow enough bandwidths [19, 20], or from pronounced Fe–Fe interactions considered possible across the shared faces of FeS_6 octahedra along the c-axis [21]. The non-metallic and diamagnetic state of the monoclinic phase at $P > 7$ GPa is consistent with a fully occupied t_{2g}-derived valence band structure as a result of spin-pairing to yield a low-spin 3d : $t_{2g}^6\, e_g^0$ electronic configuration having quenched atomic spin $S = 0$, depicted in figure 7(c).

Previous high-pressure x-ray diffraction structural studies at room temperature [8] have shown that from ambient pressure up to ∼7 GPa, preceding the structural transition to the monoclinic phase, there is a ∼10% reduction in unit-cell volume V and an additional ∼5% reduction at the transition. Since $\Delta_{cf} \propto V^{-5/3}$, derived from the inverse fifth power dependence of Δ_{cf} on average Fe–S interatomic distance [18], we anticipate that a 10% reduction in unit-cell volume alone for FeS would increase Δ_{cf} by ∼20% from an ambient estimate of ∼1.6 eV [18] up to ∼1.9 eV at ∼7 GPa. At pressure, Δ_{ex} may be anticipated to decrease from its ambient estimate of 1.7–2.0 eV [18] due to increased cation–ligand orbital mixing. Thus the reduction in unit-cell volume up to modest pressures of ∼7 GPa may quite plausibly lead to the spin-crossover condition $\Delta_{cf} \geqslant \Delta_{ex}$, invoking the electronic change depicted in the sequence from figure 7(b) to figure 7(c) with an energy gap of ε as shown in figure 7(c) for the monoclinic phase. This energy gap proposed here to be between the minority-spin $t_{2g}(\downarrow)$ and majority-spin $e_g(\uparrow)$ sub-bands is different in origin from the gap in figure 7(b) for the troilite and MnP/hexagonal phases which we propose originates from the strong electron correlation within the minority-spin $t_{2g}(\downarrow)$ sub-band.

4.2. Band magnetism and the magnetic–electronic property of Fe_7S_8

In contrast to the antiferromagnetic non-metallic behaviour observed in FeS at ambient conditions and under pressure, the behaviour in Fe_7S_8 at ambient conditions and also at

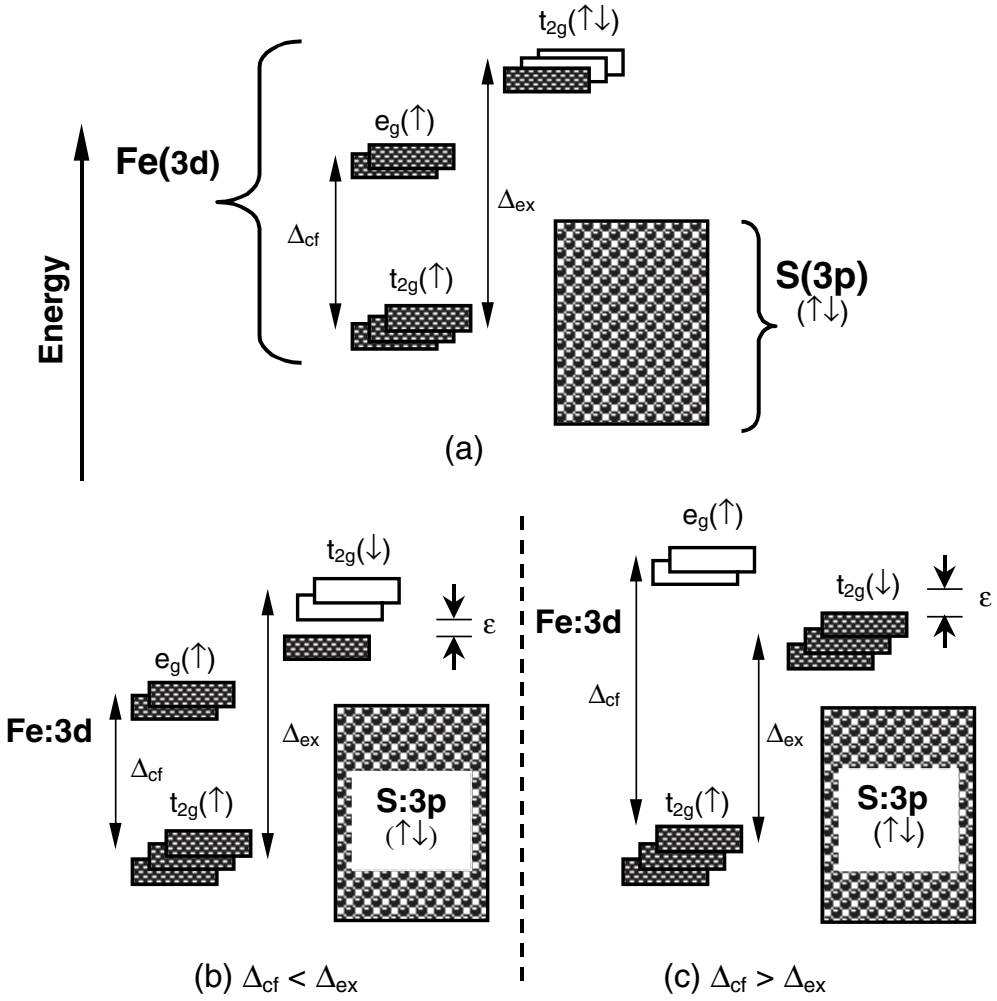

Figure 7. Schematic of the possible band structure for FeS for various electronic configurations: (a) metallic high-spin state as expected from conventional band theory, (b) high-spin state with semiconducting gap ε and (c) semiconducting low-spin state. Shaded rectangles are the highest occupied Fe:3d and S:3p bands. In the case of (b) and (c), the effect of on-site Coulomb repulsion, the Hubbard U, is implicitly included, possibly giving rise to the gap ε. Shaded 3d electronic states then represent lower (occupied) Hubbard sub-bands.

pressure (see figures 2 and 4) is different in that it is ferrimagnetic and metallic. The structural response under pressure is also in contrast to that of FeS, there being no structural symmetry change that was observed in FeS to accompany the magnetic phase transition [6]. These suggest a collective electron model and associated itinerant magnetism as being more appropriate to describe this system [4].

In this band or itinerant electron model the condition for a stable magnetism is determined by the Stoner criterion, $KN(E_F) > 1$ for a stable magnetic state to occur, where K is the Stoner integral and $N(E_F)$ is the density of state at the Fermi level. First-principles electronic band structure calculations using the linearized augmented plane-wave method [22] show that the electronic band structure of Fe_7S_8 in the magnetic state is considerably altered from that in the

non-magnetic state due to a large (∼3.2 eV) exchange splitting of the 3d band. It is suggested that the density of states at the Fermi level under pressure is reduced remarkably compared with that at ambient conditions. Therefore, the collapse of magnetism in Fe_7S_8 at ∼5 GPa is perhaps best ascribed to the pressure-induced breakdown of the Stoner criterion within a collective electron model of magnetism applicable to this system. The magnetic property observed at low pressures then signifies the condition that the density of states is high enough to sustain the magnetism.

To satisfy the charge neutrality condition pyrrhotite-Fe_7S_8 may be formulated as $[(Fe^{2+})_5(Fe^{3+})_2\square](S^{2-})_8$, where □ denotes an Fe vacancy, suggesting two charge states for Fe. The Fe^{3+} charge state would be the result of the temporary residence time of an electron hole h^+ at an Fe^{2+} site, i.e., as $(Fe^{2+}h^+)$. Hole hopping amongst the iron 3d orbitals then accounts for the metallic behaviour in this dual charge-state model. An alternative formulation may well be $[(Fe^{2+})_7\,\square][(S^{2-})_8(h^+)_2]$, corresponding to charge depletion in orbitals mainly centred on sulfur giving rise to a metallic state due to hole conduction within the S:3p band [10].

Our analyses of the spectra in figure 2 show that the isomer shifts for all sub-spectra are the same (∼0.64 mm s^{-1}) at ambient conditions, and ∼0.40 mm s^{-1} at 11.3 GPa, respectively, with respect to metallic iron. The quadrupole-interaction doublets in figures 2(c) and (d) associated with the different Fe local environments in the metal-full and metal-deficient layers of the structure all have the same isomer shift at a particular temperature in the magnetic low-pressure phase and also in the diamagnetic high-pressure phase. This signifies that Fe is in a single valence state within the $\sim 10^{-8}$ s sensing time (given by the inverse of the nuclear Larmor precession frequency in the magnetic state and the nuclear lifetime in the diamagnetic state) associated with the Mössbauer transition, even at the lowest temperature of 10 K.

Hole hopping amongst Fe:3d orbitals, and concomitant semi-metallic or metallic behaviour, may well be very rapid at high temperatures so that discrete Fe charge states may not be discerned. However, at low temperatures these holes are expected to be firmly bound to the vacancies so that most of them would be stationary for a relatively long period and distinct charge states, nominally as Fe^{2+} and $(Fe^{2+}h^+ = Fe^{3+})$, should be evident. The very similar isomer shifts for the components in the spectra at low temperatures in the high-pressure phase (e.g., figure 2(d)) do not support the notion of distinct Fe charge states, in spite of increased orbital overlap under pressure. Therefore hole conduction associated with the S:3p band is a more likely scenario that may describe the nature of vacancy states associated with the deficient iron sites.

Acknowledgment

The authors acknowledges financial support from the University of the Witwatersland and the National Research Foundation-NFR (Pretoria).

References

[1] Williams Q and Jeanloz R 1990 *J. Geophys. Res.* **95** 19 299
[2] Evans H T Jr 1970 *Science* **167** 621
[3] Horwood J L, Townsend M G and Webster A H 1976 *J. Solid State Chem.* **17** 35
[4] Shimada K, Mizokawa T, Mamiya K, Saitoh T, Fujimori A, Ono K, Kakizaki A, Ishii T, Shirai M and Kamimura T 1998 *Phys. Rev.* B **57** 8845
[5] Fei Y, Prewitt C T, Mao H-K and Bertika C 1995 *Science* **268** 1892
[6] Kobayashi H, Sato M, Kamimura T, Sakai M, Onodera H, Kuoda N and Yamaguchi Y 1997 *J. Phys.: Condens. Matter* **9** 515
[7] King H E Jr and Prewitt C T 1982 *Acta Crystall.* B **82** 1877

[8] Kusaba K, Syono Y, Kikegawa T and Shimomura O 1998 *J. Phys. Chem. Solids* **59** 945
[9] Nelmes R J, McMahon M I, Belmonte S A and Parise J B 1999 *Phys. Rev.* B **59** 9048
[10] Ward J C 1970 *Rev. Pure Appl. Chem.* **20** 175
[11] King H, Virgo D and Mao H K 1978 *Carnegie Inst. Washington Yearbook* **77** 830
[12] Takele S and Hearn G R 1999 *Phys. Rev.* B **60** 4401
[13] Reichlin R L 1983 *Rev. Sci. Instrum.* **54** 1674
[14] Zaanen J, Sawatzky G A and Allen J W 1985 *Phys. Rev. Lett* **55** 418
[15] Bocquet A E, Mizokawa T, Saitoh T, Namatame H and Fujimori A 1992 *Phys. Rev.* B **46** 3771
[16] Goodenough J B 1971 *Mat. Res. Bull.* **6** 967
[17] Hüfner S 1994 *Adv. Phys.* **43** 183
[18] Burns R G 1993 *Mineralogical Applications of Crystalfield Theory* (Cambridge: Cambridge University Press)
[19] Goodenough J B 1972 *J. Solid State Chem.* **5** 144
[20] Satpathy S, Popovic Z S and Vukajlovic F R 1996 *Phys. Rev. Lett.* **76** 960
[21] Goodenough J B 1980 *J. Solid State Chem.* **33** 219
[22] Shirai M, Suzuki N and Motizuki K 1996 *J. Electron Spectrosc. Relat. Phenom.* **78** 95